



Temperature-induced structural change through the glass transition of silicate glass by neutron diffraction

Ying Shi ^{1,*}, Ozgur Gulbiten,¹ Jörg Neufeind ², Dong Ma,³ Albert P. Song,⁴ Bryan Wheaton,¹ Mathieu Bauchy,⁵ and Stephen R. Elliott⁶

¹*Science and Technology Division, Corning Incorporated, Corning, New York 14831, USA*

²*Neutron Scattering Division, Spallation Neutron Source, Oak Ridge National Laboratory, Oak Ridge, Tennessee 37831, USA*

³*Neutron Science Platform, Songshan Lake Materials Laboratory, Dongguan, Guangdong 523808, China*

⁴*Corning-Painted Post High School, Corning, New York 14830, USA*

⁵*Physics of Amorphous and Inorganic Solids Laboratory (PARISlab), Department of Civil and Environmental Engineering, University of California, Los Angeles, California 90095, USA*

⁶*Department of Chemistry, University of Cambridge, Lensfield Road, Cambridge CB2 1EW, United Kingdom*



(Received 23 December 2019; revised manuscript received 16 March 2020; accepted 16 March 2020; published 16 April 2020)

Supercooled silicate liquids exhibit several orders of magnitude increase in viscosity at the glass-transition temperature (T_g) towards the glassy state. Such a drastic dynamical slowdown leads to an abrupt change in the slope of temperature-dependent thermodynamic properties because the measurements reflect the equilibrium-to-nonequilibrium change from liquid to glass. However, an underlying structural change associated with such a transition remains elusive. For instance, understanding the structural origin of the variation in the coefficient of thermal expansion (CTE) of silicate glasses upon vitrification is critical for glass-manufacturing processes and applications. Here, based on temperature-dependent neutron diffraction, we demonstrate that the temperature dependences of both short- and medium-range order structural parameters show a pronounced change of slope at T_g for a range of silicate glasses of industrial importance. Interestingly, the short- and medium-range order structural parameters are found to be mutually correlated, both below and above T_g . Based on these results, we find that the slope change of the area of the first sharp diffraction peak at T_g is correlated with the extent of the CTE jump at T_g , which offers a structural origin for the discontinuity in the CTE of glasses at T_g . This study can therefore shine light on solving critical industrial problems, such as glass relaxation.

DOI: [10.1103/PhysRevB.101.134106](https://doi.org/10.1103/PhysRevB.101.134106)

I. INTRODUCTION

The glass transition is one of the most challenging topics in condensed-matter physics [1]. When a supercooled liquid is cooled below the glass-transition temperature (T_g) into the glassy state, its viscosity suddenly increases by several orders of magnitude. Meanwhile, experimentally measured macroscopic properties, such as the specific heat capacity [2] and the coefficient of thermal expansion (CTE) [3], show a continuous but abrupt decrease—i.e., a change of slope through T_g . Such an abrupt change is a consequence of the drastic dynamical slowdown experienced by supercooled liquids as they approach the glassy state. The properties measured for the above- T_g supercooled liquid are representative of the metastable equilibrium state, that is, wherein the measurement time is much longer than the structural relaxation time. In contrast, the properties measured for the below- T_g glassy state reflect the nonequilibrium state, since the experimental measurement time is much shorter than the structural relaxation time of the glass. If, by a thought experiment, one could measure the equilibrium thermodynamic properties of the

below- T_g glassy state, which means that a virtually infinite time would be allowed for the glass to reach its equilibrium state, one would expect no slope change in the temperature dependence of a property measured around T_g . Nevertheless, measurements of below- T_g nonequilibrium properties are very crucial as they capture the true out-of-equilibrium nature of glasses used for effectively all the practical applications in everyday life. Moreover, the through- T_g slope change of the temperature dependence provides even more critical information because it reflects the underlying configurational structural change from a nonequilibrium to an equilibrium state [3], which, in turn, governs the low-temperature glass-relaxation behavior but cannot be directly measured.

The microscopic structural manifestation of the glass transition has been observed in other materials than silicate glasses. In detail, a slope change of the temperature dependence of the first sharp diffraction peak measured by elastic neutron scattering has been reported for polymers [4]. A similar slope change has also been observed for the mean-square atomic displacement, i.e., the Debye-Waller factor ($\langle u^2 \rangle$), in polymers and glassy selenium [5] based on inelastic neutron scattering [5], and in amorphous proteins by Mössbauer scattering [6]. All these materials exhibit a high fragility, that is, the viscosity exhibits a very pronounced variation in the

*shiy3@corning.com

TABLE I. Description of four silicate glasses, the glass-transition temperature T_g , density, the maximum temperature for neutron measurement, and number of collected diffraction patterns.

Glass I.D.	Description	T_g (°C)	Density (g/cm ³)	T_{\max} (°C)	No. of patterns
FS	SiO ₂	1140	2.199	950	16
CG	Mixed alkaline aluminosilicate [23]	677.4	2.416	825	13
NIST 710a	Soda-lime silica [24]	551.5	2.544	660	13
Jade [®]	Mixed alkaline earth aluminosilicate [3]	802.2	2.629	950	15

vicinity of T_g . This leads to large through- T_g slope changes for experimentally measured macroscopic thermodynamic properties, and, consequently, relatively large changes of the underlying microscopic structure. Here, we investigate the through- T_g structural change of industrially important silicate glasses, which present a much lower fragility (i.e., stronger behavior) as compared to polymer materials.

The CTE of silicate glasses often increases by a factor of 2–3 times through T_g [3]. However, no clear microscopic structural signature of the glass transition in silicate glasses has thus far been found. A number of *in situ* high-temperature, diffraction studies of oxide glasses [7–9] have concentrated on the structural changes occurring between room-temperature (RT) glass and high-temperature melt. There are, however, a few *in situ* studies reporting measurements around T_g , in particular for potassium disilicate [10], soda-lime silicate [11] glasses by neutron diffraction, and for fused silica (FS) [12], CaSiO₃ [13], CaAl₂O₄ [14], and BaTi₂O₅ [15] glasses by x-ray diffraction. However, none of those studies has revealed any clear structural signature for the abrupt change in some macroscopic physical properties at T_g . Therefore, it is often inferred that, for silicate glasses [10,11], only subtle structural changes occur at the glass-transition temperature, and consequently glasses are often considered as simply being “structurally frozen liquids.”

On the other hand, remarkable progress has been made in understanding the kinetics and thermodynamic properties of glass-forming liquids [5,6]. Macroscopic measurements and theoretical approaches have searched for the origins of the complex dynamics of the equilibrium-to-nonequilibrium transition [16,17], which is intimately related to the nonexponential [18] and nonlinear [19] nature of structural-relaxation processes in glasses. Structural relaxation is also a critical and compelling topic in the display-glass industry [20], so that an understanding of the structural origins of glass relaxation might help solve industrial problems, in addition to answering fundamental physics questions. Since the supercooled liquid-to-glass transition arises when the relaxation time exceeds the observation time [21], elucidation of the structural changes occurring in silicate glasses through the glass transition might shine light on the origin and mechanism of relaxation in glasses.

Recently, we demonstrated an analytical method to elucidate the continuous short-range and medium-range structural change of fused silica at temperatures below the glass-transition temperature using *in situ* neutron total scattering [22]. In this study, we elaborate on the structural variations occurring in the vicinity of the glass transition in three industrially important silicate glasses from *temperature-dependent* neutron-diffraction data. We find that both short- and medium-

range order structural parameters show a signature of the glass transition. Applying the method developed in Ref. [22], the short-range structural information is derived from the nearest Si-O and O-O atom pairs of the pair-distribution function in real space. The medium-range structural information is derived from the area of the first sharp diffraction peak (FSDP) of the structure factor in reciprocal space. Despite the different length scales which they reflect, the temperature dependences of these structural parameters are found to be mutually correlated, both below and above T_g . Furthermore, we find that the magnitude of the CTE jump at T_g is correlated to the slope change of the FSDP area at T_g , which establishes a structure–property relationship.

II. METHODS

A. Glasses

In addition to the prototypical fused silica glass, three other silicate glasses were chosen for *in situ* high-temperature neutron-diffraction measurements to explore structural changes through T_g . These glasses cover a wide range of values of CTE jumps, with $CTE_{\text{liquid}}/CTE_{\text{glass}}$ ratios varying from 2 to 3.5. As listed in Table I, two are aluminosilicate glasses: CG contains a mixture of alkaline oxides [23], while Jade[®] contains alkaline-earth oxides [3]. NIST 710a is a mixed alkaline and alkaline-earth silicate glass [24]. T_g values were determined from an equilibrium three-point beam-bending viscosity measurement method [25], employing Angell’s definition of T_g , which is the temperature when the equilibrium viscosity equals 10^{12} Pa s [6].

B. *In situ* neutron-diffraction measurements

Time-of-flight neutron-diffraction measurements were performed on the Nanoscale-Ordered Materials Diffractometer (NOMAD) at the Spallation Neutron Source, Oak Ridge National Laboratory [26]. Glasses were core drilled into 6-mm-diameter and 24-mm-long rods and loaded into a vanadium can. The rods were heated in an ILL furnace with a 5 °C/min ramp rate by following a staircase profile from room temperature to 100–150 °C above the particular T_g temperature (except for FS). The furnace-temperature control error was ± 5 °C. At each data-collection temperature, the sample was held isothermally for 25 min, which includes 5 min of hold time followed by 20 min of data collection. First of all, a room-temperature scan was conducted. Then, for temperatures below T_g , 20-min scans were performed at every 150 °C interval. Above T_g , data collection was performed at 10–25 °C intervals from T_g to ~ 200 °C above T_g (except for FS). The T_g temperature itself was intentionally skipped because

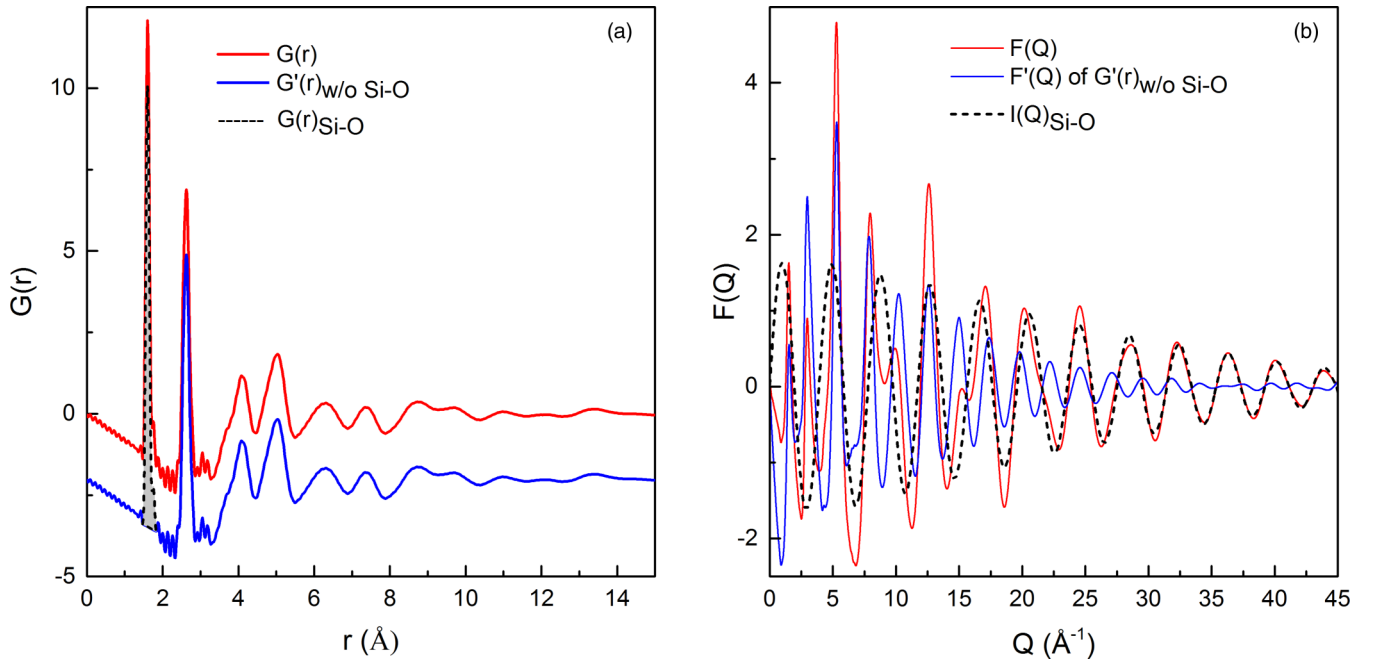


FIG. 1. Reciprocal-space $I(Q)$ obtained by Fourier transformation of $G(r)_{\text{Si-O}}$ for fused silica. (a) Real space: original $G(r)$ (red); $G'(r)$ with first Si-O pair subtracted (blue); $G_{\text{Si-O}}(r)$ (black), both blue and black curves are shifted down by 2 for clarity. (b) Reciprocal space: $F(Q)$ of original $G(r)$ (red); $F'(Q)$ of $G'(r)$ (blue); $I(Q)$ of first Si-O pairs (black), where $I(Q) = F(Q) - F'(Q)$.

the relaxation times are similar to the neutron-measurement timescales in the vicinity of the glass-transition temperature. Therefore, only the below- T_g nonequilibrium and above- T_g equilibrium data are used to study the through- T_g structural change. All the measured neutron structure factors obtained in this study were normalized to an absolute scale, utilizing the low- r region of $G(r)$ criterion, as described in Ref. [27]. The statistical errors of the neutron structure factors measured by this *in situ* setup and the Fourier-transform propagation errors of the pair-distribution function are shown in Ref. [22].

C. Reciprocal-space representation of intratetrahedral bonds- $I_{\text{Si-O}}(Q)$ and $I_{\text{O-O}}(Q)$

The detailed procedure to derive the reciprocal-space representation, $I(Q)_{i-j}$ for $i-j$ atom pairs in $G(r)$ is illustrated in Ref. [22]. Here, we demonstrate how to obtain $I_{\text{Si-O}}(Q)$ for the nearest Si-O atom pairs. As shown in Fig. 1(a), $G(r)$ (red curve) can be decomposed into two additive components: the Si-O nearest-neighbor peak itself, shown in black, and everything else, denoted as $G'(r)$ and shown in blue. Fourier transformation of $G(r)$ and $G'(r)$ leads to the corresponding reduced structure factors, $F(Q)$ and $F'(Q)$, with $F(Q) = \int_0^{Q_{\text{max}}} G(r) \sin(Qr) dr$. As shown in Fig. 1(b), $I_{\text{Si-O}}(Q)$ is the difference between $F'(Q)$ and $F(Q)$, shown as the black dotted curve. It is mathematically equivalent to the direct Fourier transformation of the nearest-neighbor Si-O atom pairs. We need to apply this procedure because our Fourier-transformation algorithm only allows us to compute the Fourier transformation of $G(r)$ over the entire range of r values rather than over the extent of the individual single peaks of $G(r)$.

III. RESULTS

A. *In situ* high-temperature neutron-diffraction data

The reduced structure factors, $F(Q)$ (where $F(Q) = Q[S(Q) - 1]$), of the four silicate glasses as a function of temperature are presented in Fig. 2. All the four glasses exhibit typical thermal-vibration effects, that is, all the peaks

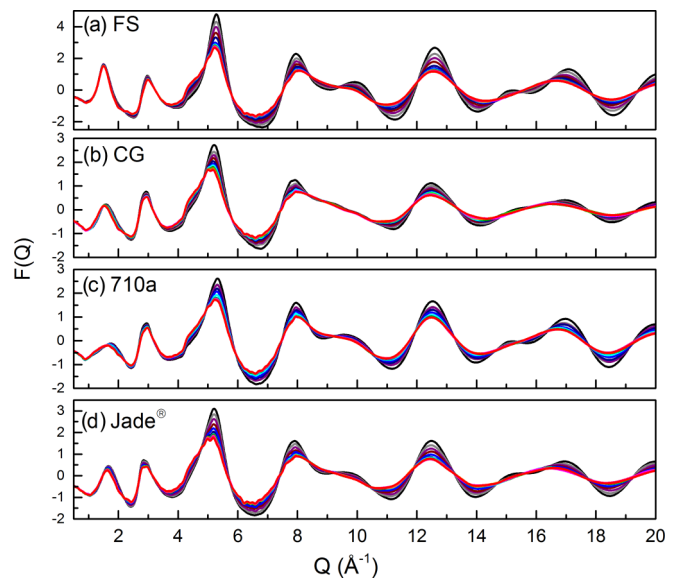


FIG. 2. Reduced structure factor functions $F(Q)$ of four silicate glasses measured from room temperature up to 150 °C above each specified T_g (except for FS). The RT $-F(Q)$ is plotted in black, then the color changes following the rainbow color spectrum, until the highest temperature $F(Q)$ is plotted in red.

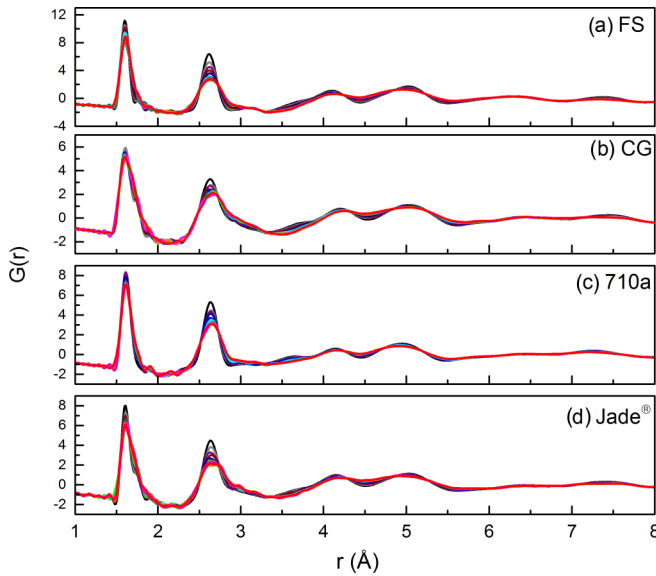


FIG. 3. The reduced pair-distribution functions $G(r)$ ($Q_{\max} = 50 \text{ \AA}^{-1}$) of four silicate glasses from room temperature up to 150°C above each specified T_g (except for FS). The same color scheme is used as in Fig. 2.

become broader and their intensities decrease with increasing temperature. The extent of the changes increases with Q^2 , as expected for atomic correlations exhibiting a Debye-Waller behavior [28].

The reduced pair-distribution functions $G(r)$ are obtained by direct Fourier transformation of $F(Q)$, with $G(r) = (\frac{2}{\pi}) \int_0^{Q_{\max}} F(Q) \sin(Qr) dQ$ ($Q_{\max} = 50 \text{ \AA}^{-1}$). As shown in Fig. 3, all the peaks broaden with increasing temperature. The first peak, representing the nearest A-O pairs (where A represents the glass formers Si and Al), is increasingly non-Gaussian and asymmetric with a long- r tail.

B. Short-range structural change

The short-range temperature-dependent structural change, i.e., the AO_4 tetrahedra expansion, is reflected in the change of the first two peaks of $G(r)$, that is, the nearest-neighbor A-O and O-O correlations. To derive accurate structural information, we choose to work with the reciprocal-space representation of atom-pair correlations since it expands the signal and allows for more reliable model fitting, as demonstrated in our RingFSDP method [29].

For the following analysis, we ignore the non-Gaussian asymmetry of the atom-pair correlations. This Gaussian-distribution assumption allows for a stable fit of $I(Q)_{i-j}$ with sufficient structural evolution information. For an atomic pair, ij , with a Gaussian distribution of a mean distance r_{ij} and a root-mean-square (rms) deviation in distance, $\langle u_{ij}^2 \rangle^{1/2}$, its contribution to the reduced total structure factor, $I_{ij}(Q)$, is represented by Eq. (1) [30]:

$$I_{ij}(Q) = \frac{n_i^j \times B_{ij}/c_i}{r_{ij}} \sin(r_{ij}Q) \exp(-Q^2 \langle u_{ij}^2 \rangle / 2), \quad (1)$$

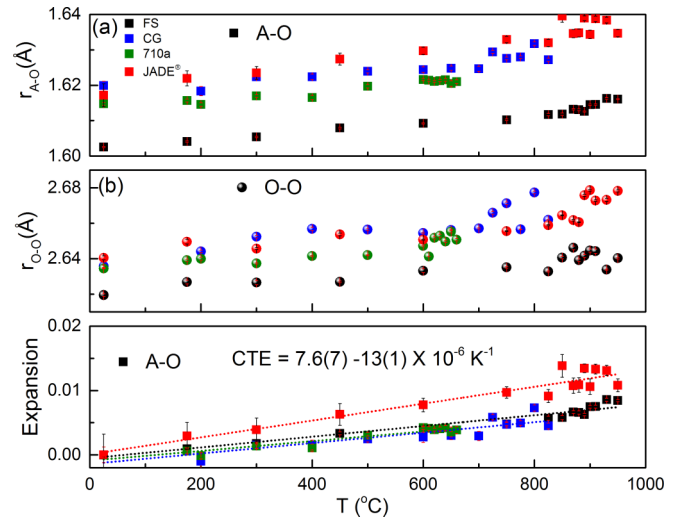


FIG. 4. Temperature dependence of A-O ($A = \text{Si}$ or Al) (a) and O-O (b) atom-pair distances determined by $I(Q)$ fitting and A-O expansions with temperature (c). The fitting-error bar is smaller than the symbol size. The CTE slopes (dotted lines) are determined by a linear fit of the whole temperature-range expansion data for each glass.

where n_i^j is the coordination number, which is the number of atoms of type j around atoms of type i , $B_{ij} = \frac{c_i c_j b_i b_j}{(\sum c_i b_i)^2}$ with c_i and b_i being the atomic fraction and neutron-scattering length of chemical species i , respectively. The quantity r_{ij} is the mean value of the interatomic distance between atom pairs i - j , and $\exp(-Q^2 \langle u_{ij}^2 \rangle / 2)$ is the Debye-Waller factor, with $\langle u_{ij}^2 \rangle$ being the mean-square deviation of the interatomic distance.

We applied this method to the *in situ* data for the four silicate glasses. A good fit was obtained for all the glasses at all temperatures, with an adjusted r^2 value in the range of 0.98–0.99. We tested using two atom-pair distances, Si-O and Al-O, for the $I_{A-O}(Q)$ fitting of the two aluminosilicate glasses, but failed to obtain a reliable fit because the difference in Si-O and Al-O bond lengths is less than a peak width. Instead, robust fitting can be attained by using average A-O and O-O atom-pair distances and an average value of B_{ij} .

The A-O and O-O atom-pair distance changes with temperature are illustrated in Figs. 4(a) and 4(b). The average distances do not show a clear change in trend through the glass transition.

Likewise, the mean-square atom-pair distance deviations of $\langle u_{A-O}^2 \rangle$ and $\langle u_{O-O}^2 \rangle$, derived from fits of $I_{A-O}(Q)$ and $I_{O-O}(Q)$, for the four silicate glasses, are displayed as a function of temperature in Fig. 5, and also do not show a clear trend through the glass transition.

Local coefficients of thermal expansion (CTE), derived from the expansion of A-O atom-pair distances, $Expansion_T = \frac{r_T - r_{RT}}{r_{RT}}$, are in the range of $7.6(7) - 13(1) \times 10^{-6} (\text{K}^{-1})$, in line with the local CTE values of soda-lime silicate glass [$6(1) \times 10^{-6} \text{ K}^{-1}$] [11] and potassium disilicate glass [$9(1) \times 10^{-6} \text{ K}^{-1}$] [10], both determined from Si-O atom-pair distance changes measured by neutron diffraction. Not surprisingly, the local CTEs show no correlation with bulk CTEs since we should not expect the local view to represent

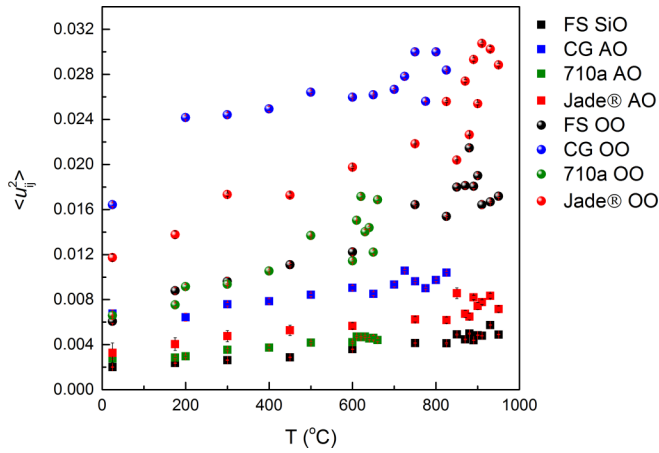


FIG. 5. Mean-square atom-pair deviation $\langle u_{ij}^2 \rangle$ changes with temperature. The fitting-error bar is about the same scale as the symbol size.

the global view. However, we are interested in exploring if the change of local view reflects the change of the global view.

In the following, we now plot structural parameters normalized by their value at T_g as a function of the scaled temperature T/T_g , which is an analog of the Oldekop-Laughlin-Uhlmann-Angell (OLUA) format [31] adopted by Ngai [5]. The OLUA type of plot is an excellent way to represent a glass-property change with temperature; it also allows one to compare glasses with different values of T_g . The analog OLUA plots for $\langle r_{ij} \rangle_T / \langle r_{ij} \rangle_{T_g}$ and $\langle u_{ij}^2 \rangle_T / \langle u_{ij}^2 \rangle_{T_g}$ with T/T_g for A-O and O-O atom pairs are shown, respectively, in Figs. 6 and 7. FS glass is excluded here because it could not be measured through its T_g value of 1140 °C, as this is outside the temperature range of the furnace used. A sudden change in slope is observed at T_g for all four plots. The glasses were not measured at their exact T_g temperatures because the relaxation times are similar to the neutron-measurement timescales in the vicinity of the glass-transition temperature. Instead, the structural parameters at T_g used as the reference point for the

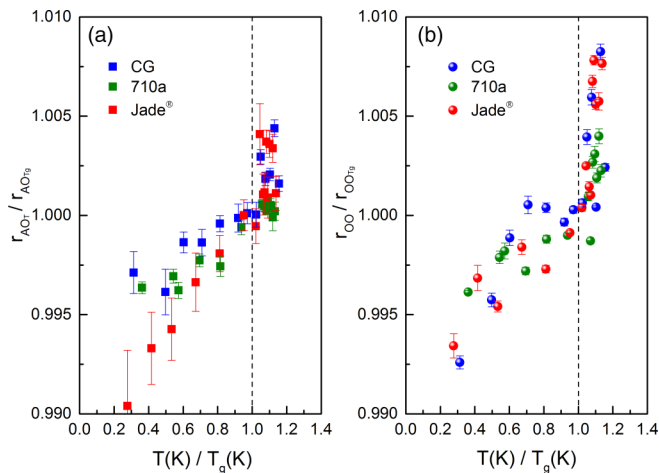


FIG. 6. An analog OLUA plot of scaled atom-pair distance r_{ijT} / r_{ijT_g} for A-O (a) and O-O (b) atom pairs as a function of scaled temperature, T/T_g . Note the significant discontinuous increase of r_{ijT} / r_{ijT_g} on passing through T_g . The error bars have been propagated from the fitting error.

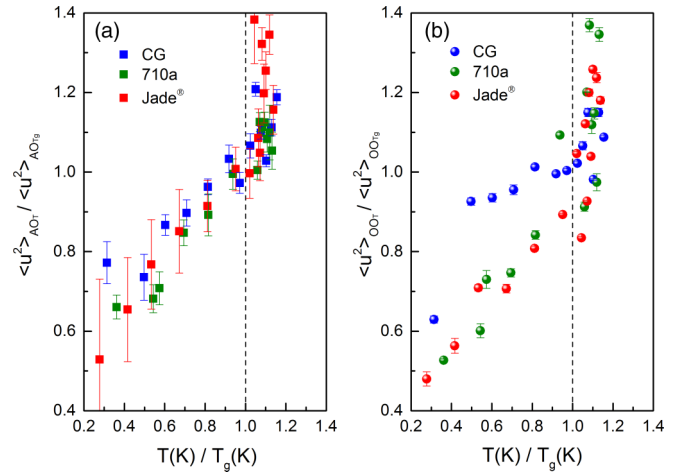


FIG. 7. An analog OLUA plot of scaled mean-square atom-pair deviation $\langle u_{ij}^2 \rangle_T / \langle u_{ij}^2 \rangle_{T_g}$ for A-O (a) and O-O (b) atom pairs as a function of scaled temperature, T/T_g . Note the significant discontinuous increase of $\langle u_{ij}^2 \rangle_T / \langle u_{ij}^2 \rangle_{T_g}$ on passing through T_g . The error bars have been propagated from the fitting error.

analog OLUA plots were interpolated from the values of their two nearest measured temperatures.

It is to be noted that we also did a direct Gaussian peak fitting of $T(r)[T(r) = 4\pi r \rho_0 + G(r)]$ for all the datasets. As shown in Fig. 8, the direct-fitting analog OLUA plots of both r_{ij} and $\langle u_{ij}^2 \rangle$ for A-O atom pairs show the same sudden slope changes at T_g , but no slope changes at T_g are observed for the analog OLUA plots for O-O atom pairs. Theoretically, fitting either a single Gaussian peak in $T(r)$ or a decaying sine wave in $I(Q)$ should provide the same structural values, r_{ij} and $\langle u_{ij}^2 \rangle$, as demonstrated for A-O atom pairs. This indicates that both of the fitting methods are capable of deriving the correct structural information and are not affected by any truncation artifacts arising from the Fourier transform, if any. The reason that direct fitting does not lead to a slope change at T_g for O-O atom pairs may be due to the O-O atom-pair correlations overlapping with those of Si-Si atom pairs, in contrast to the well-defined A-O atom pairs, as shown in Fig. 3. As demonstrated in Ref. [22], direct peak fitting produces correct mean-square atom-pair distance-deviation $\langle u_{Si-O}^2 \rangle$ values that match with reported data [32], but give two times higher $\langle u_{O-O}^2 \rangle$ values at elevated temperatures; such a discrepancy might be caused by the same overlapping reason. Therefore, the reciprocal-space $I_{ij}(Q)$ fitting should be applied for accurate structural information.

This is an experimental demonstration of a change in slope of the temperature dependence of short-range $\langle u_{ij}^2 \rangle$ parameters through T_g , and our findings are so far specific to these three silicates. However, there is some indication that this behavior may be more general. Incoherent neutron-diffraction experiments of systems as diverse as amorphous protein [6], polymers, and selenium [5] show a change of the mean-square atomic displacement $\langle u^2 \rangle$ slope at T_g . Although the mean-square atomic displacement $\langle u^2 \rangle$ is not directly related to the local mean-square displacement $\langle u_{ij}^2 \rangle$, they can be correlated. In fact, Angell [6] predicted changes in the temperature dependence of the mean-square atomic displacement $\langle u^2 \rangle$ at T_g

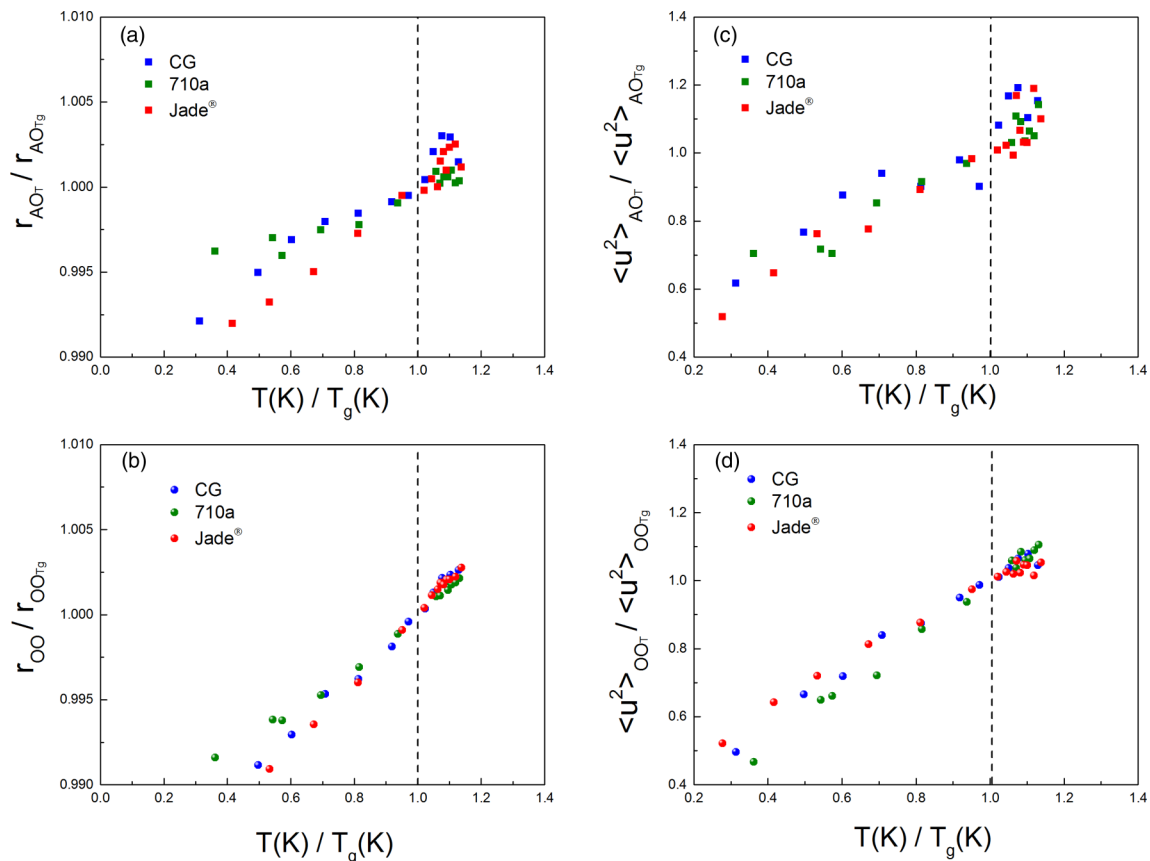


FIG. 8. Direct $T(r)$ fitting and analog OLUA plot of scaled atom-pair distance r_{ijT}/r_{ijT_g} for A-O (a) and O-O (b) and mean-square atom-pair deviation $\langle u_{ij}^2 \rangle_T / \langle u_{ij}^2 \rangle_{T_g}$ for A-O (c) and O-O (d) atom pairs as a function of scaled temperature, T/T_g . Note the sudden slope changes at T_g of both r_{ij} (a) and $\langle u_{ij}^2 \rangle$ (b) for A-O atom pairs, but no slope changes at T_g observed for the (c), (d) O-O atom pairs.

for SiO₂ and B₂O₃ glasses, but experimental evidence for this was not available at the time.

C. Medium-range structural change

The FSDP region of $F(Q)$ and the corresponding medium-range $G(r)$ curves for all four silicate glasses are plotted in Fig. 9. They are shown in the order from lowest CTE jump (FS) to the highest (Jade[®]). Qualitatively, the high-CTE-jump glass, Jade[®], shows a larger FSDP change with temperature in terms of area decrease, and shape change with the intensity dropping more on the high- Q side. We propose that the FSDP shape change could be a sign of changes of the ring shapes. The FSDP shape change has a corresponding peak change in the region of 4–5 Å in $G(r)$, as shown in Figs. 9(e)–9(h), with two peaks broadening and approaching each other. These peaks are a combination of second-nearest-neighbor Si···O and O···O atom-pair correlations [33], but need modeling work to be interpreted fully (work in progress).

We focus on the reciprocal-space $S(Q)$ -FSDP to study the medium-range structural change for all four silicate glasses. Figure 10 shows the $S(Q)$ -FSDP area change with temperature. As discussed previously [29], we determine a linear background in $F(Q)$, since $F(Q)$ has very well-defined minima

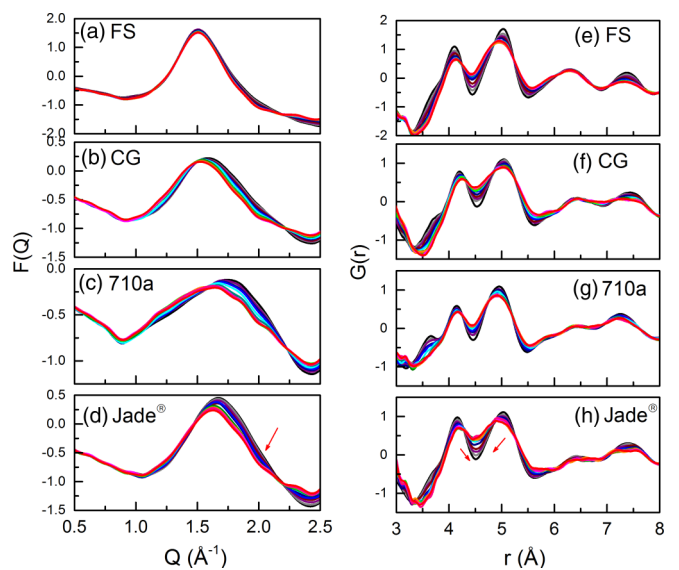


FIG. 9. The FSDP region of $F(Q)$ and its corresponding medium-range $G(r)$ of four silicate glasses measured from room temperature up to 150 °C above each specified T_g (except FS). The same color scheme is used as in Fig. 2. Note the FSDP shape change, which skews more to low Q , as shown by the arrow. Also note the abnormal peak change in the region of 4–5 Å in $G(r)$.

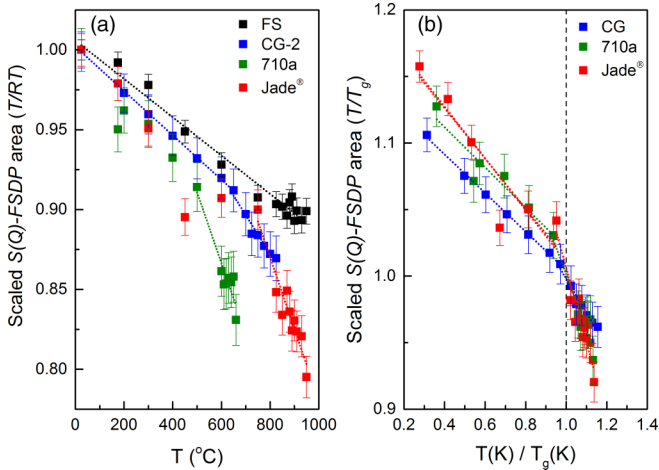


FIG. 10. $S(Q)$ -FSDP area drop with T . (a) $S(Q)_T$ -FSDP scaled by the RT value as a function of T for all four glasses. (b) $S(Q)_T$ -FSDP scaled with T_g values as a function of scaled $T(T/T_g)$ for three glasses except FS. The error bars are calculated from the $S(Q)$ -FSDP area integration error which is propagated from the $S(Q)$ counting statistics error.

on both sides of the FSDP maximum, and we integrate the $S(Q)$ -FSDP area above the background converted from the $F(Q)$ -determined linear background. In Fig. 10(a), the $S(Q)$ -FSDP area is scaled by the RT value; all glasses, including FS, show a similar negative slope below T_g with good linearity, and a steep drop for the three silicate glasses at their corresponding T_g values. The OLU plot, $S(Q)$ -FSDP area change scaled by T/T_g vs T/T_g for three glasses except FS, is shown in Fig. 10(b). A clear change in slope is observed for all glasses at $T/T_g = 1$. This establishes the $S(Q)$ -FSDP area as another structural signature of the glass transition. A similar observation was reported for a metallic glass that the slope of the height of the first peak of $S(Q)$ versus temperature shows a steep drop at T_g [34]. Again, this indicates a more general behavior, not only specific to silicate glasses.

Intriguingly, as listed in Table II and plotted in Fig. 11, it is observed that the ratios between the supercooled-liquid and glass slopes for the $S(Q)$ -FSDP area change with T are proportional to the dilatometrically measured CTE ratios above and below T_g . This demonstrates that we have found a microscopic structural fingerprint that is correlated with the trend of the macroscopic properties when a glass is heated above the glass transition. The good linear correlation ($R^2 = 0.97$) between

TABLE II. CTE values measured by dilatometry, in comparison with the slope of the $S(Q)$ -FSDP area drop for slope_g, slope_l, and their ratio (slope_l/slope_g). The estimated errors for dilatometry CTE measurements are 0.25 and $0.5 \times 10^{-6}/\text{K}^{-1}$ for glass and liquid, respectively. The error in the slope for the $S(Q)$ -FSDP area change is determined from linear fitting. The errors for the liquid/glass ratio for CTE and slope are calculated by error propagation.

Glass I.D.	Dilatometry			FSDP $S(Q)$ area		
	CTE _{glass} ($\times 10^{-6} \text{K}^{-1}$)	CTE _{liquid} ($\times 10^{-6} \text{K}^{-1}$)	CTE ratio (liquid/glass)	Slope _{glass} (K^{-1})	Slope _{liquid} (K^{-1})	Slope ratio (liquid/glass)
FS	0.55			-0.120(4)		
CG	8.86	20.18	2.28(8)	-0.143(2)	-0.25(2)	1.8(1)
710a	8.81	27.25	3.1(1)	-0.15(1)	-0.40(4)	2.7(3)
Jade®	4.23	14.65	3.5(2)	-0.19(2)	-0.56(5)	3.0(4)

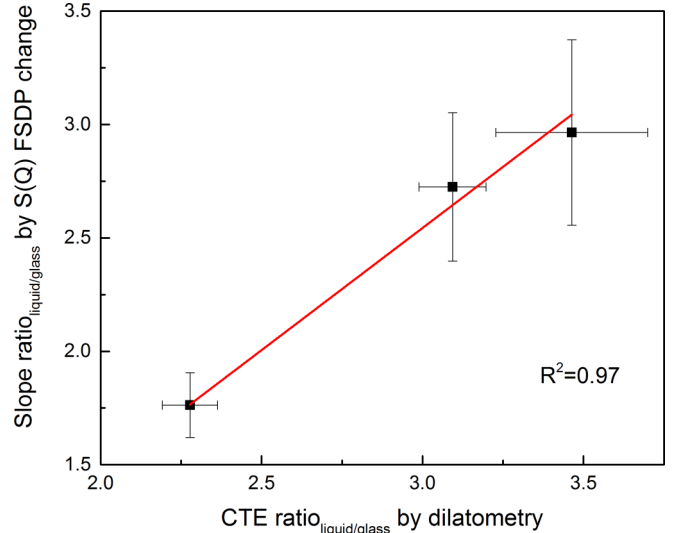


FIG. 11. Correlation between a structural parameter measured by neutron diffraction and through- T_g bulk CTE changes measured by dilatometry. A positive linear correlation is observed between the $S(Q)$ -FSDP area slope ratio (supercooled liquid vs glass) and the bulk CTE ratio (supercooled liquid vs glass).

the change in the microscopic quantity of the $S(Q)$ -FSDP area and the macroscopic bulk CTE is shown in Fig. 11. This is probably the key result of this study, as it establishes a clear structure–property relationship.

D. Correlation between short- and medium-range structural change

Since the temperature dependences of both short- and medium-range structural parameters show a change of slope at T_g , it is reasonable to ask to what extent these parameters are correlated. Figure 12 shows the T_g -scaled bond distance r_{A-O} (a) and Debye-Waller parameter $\langle u_{A-O}^2 \rangle$ (b) against the FSDP area. A linear correlation is found ($R^2 = 0.77$ for r_{A-O} and $R^2 = 0.82$ for $\langle u_{A-O}^2 \rangle$) from the combined data of three glasses and it establishes a connection between the short- and medium-range structural changes.

Although this is not totally surprising, we want to further understand, maybe somewhat speculatively, how these two different length scales are connected. The mutual reorganization of AO_4 rigid units ($A = \text{Si}$ and Al) was identified as being the origin of structural changes for both crystalline

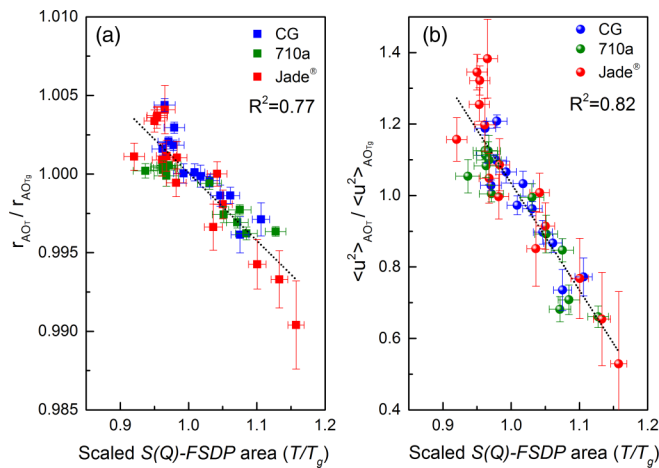


FIG. 12. Inverse linear correlations between T_g -scaled short- and medium-range structural parameters by fitting all three silicate glasses data. (a) Correlation between T_g -scaled r_{A-O} and $S(Q)$ -FSDP area; (b) Correlation between T_g -scaled $\langle u_{A-O}^2 \rangle$ and $S(Q)$ -FSDP area.

[35,36] and glassy [37] silicate materials, where A - O - A rotations between AO_4 rigid units, including both bond-angle and dihedral- (torsion-) angle changes, only requires small energy barriers to be overcome. The medium-range, reciprocal-space FSDP reflects the ring structure [29]. The short-range metrics r_{ij} and $\langle u_{ij}^2 \rangle$ are derived from the real-space nearest A - O and O - O atom pairs which form the basic AO_4 building block. The A - A atom-pair distance and deviation, r_{A-A} and $\langle u_{A-A}^2 \rangle$ have the most direct connection to the A - O - A rotations. However, the A - A parameters cannot be determined reliably from neutron-diffraction data because of the small scattering length of Si or Al relative to O. Since all the atoms are connected with each other, the values of A - A pairs are closely correlated to other atom pairs and the A - O and O - O atom pairs are reasonably good proxies for the A - A parameters and hence the A - O - A angle. This allows us to use r_{A-O} and $\langle u_{A-O}^2 \rangle$ to represent the extent of A - O - A rotations, although these parameters do not seem to have a direct correlation. Consequently, the increase of r_{A-O} and $\langle u_{A-O}^2 \rangle$ with temperature can lead to a high degree of A - O - A rotation and a distortion of ring shapes, which, as a result, can cause a decrease of the area of the first sharp diffraction peak. This can explain the inverse linear correlation observed in Fig. 12.

IV. CONCLUSIONS

Temperature-induced structural changes for four silicate glasses have been studied by *in situ* neutron-diffraction analysis, with special focus on the glass-transition temperature (T_g) range. The short-range structural parameters, r_{ij} and $\langle u_{ij}^2 \rangle$, normalized by their corresponding T_g values, show significant increases at T_g with pronounced changes of slope of the temperature dependence. These two values are indirectly

correlated to the extent of low-energy A - O - A rotations, which in turn represent the rearrangement of nearest-neighbor AO_4 tetrahedral units. Such rearrangements distort the ring shapes, which lead to a decrease in the $S(Q)$ -FSDP area with a steep drop at T_g . Therefore, we demonstrate that both the short-range r_{ij} and $\langle u_{ij}^2 \rangle$ and medium-range $S(Q)$ -FSDP area structural parameters capture the structural changes occurring at the glass transition. Despite the different length scales which they represent, these parameters are found to be mutually correlated through the entire temperature range investigated herein, both below and above T_g . Although r_{ij} and $\langle u_{ij}^2 \rangle$ are fundamental to a description of the short-range structure, they are more difficult to obtain compared to direct peak-area integration of the $S(Q)$ -FSDP. The correlation between the two may thus enable the characterization of silicate structures more quickly and when a full range of $S(Q)$ measurements is not possible, such as for sample environments that offer limited angular accessibility.

The datasets generated and analyzed in this study are available from the corresponding author upon reasonable request.

ACKNOWLEDGMENTS

Neutron measurements used resources at the Spallation Neutron Source, a Department of Energy (DOE) Office of Science User Facility operated by the Oak Ridge National Laboratory. Many thanks are owed to Michelle Everett for technical assistance at NOMAD and Daniel Olds (formerly at ORNL) for the PYTHON algorithm for Fourier transformation. Y.S. is grateful for constructive comments from Oliver Alderman of Materials Development Inc. M.B. acknowledges funding provided by the National Science Foundation under Grant No. 1928538.

Y.S. designed the research; Y.S., J.N., and D.M. carried out the neutron measurements; O.G. prepared the glasses; A.S. developed the PYTHON code; Y.S., J.N., D.M., O.G., B.W., M.B., and S.R.E. analyzed the data; and Y.S., J.N., O.G., M.B., and S.R.E. wrote the manuscript.

This work has been partially supported by U.S. DOE Grant No. DE-FG02-13ER41967. ORNL is managed by UT-Battelle, LLC, under Contract No. DE-AC05-00OR22725 for the U.S. Department of Energy.

The U.S. Government retains and the publisher, by accepting the article for publication, acknowledges that the U.S. Government retains a nonexclusive, paid-up, irrevocable, worldwide license to publish or reproduce the published form of this manuscript, or allow others to do so, for U.S. Government purposes. The Department of Energy will provide public access to these results of federally sponsored research in accordance with the DOE Public Access Plan [38].

PYTHON program - Tetrahedron Expansion was used to pairs and then profile fit $I(Q)$. The codes are available from the NOMAD beamline of Oak Ridge National Laboratory (ORNL) upon request [39].

- [1] G. B. McKenna, Diverging views on glass transition, *Nat. Phys.* **4**, 673 (2008).
 [2] Q. Zheng, Y. Zhang, M. Montazerian, O. Gulbiten, J. C. Mauro, E. D. Zanotto, and Y. Yue, Understanding glass through

- differential scanning calorimetry, *Chem. Rev.* **119**, 7848 (2019).
 [3] M. Potuzak, J. C. Mauro, T. J. Kiczanski, A. J. Ellison, and D. C. Allan, Resolving the vibrational and configurational contri-

- butions to thermal expansion in isobaric glass-forming systems, *J. Chem. Phys.* **133**, 091102 (2010).
- [4] B. Frick, D. Richter, and C. L. Ritter, Structural changes near the glass transition-neutron diffraction on a simple polymer, *Europhys. Lett.* **9**, 557 (1989).
- [5] K. L. Ngai, Dynamic and thermodynamic properties of glass-forming substances, *J. Non-Cryst. Solids* **275**, 7 (2000).
- [6] C. A. Angell, Formation of glasses from liquids and biopolymers, *Science* **267**, 1924 (1995).
- [7] L. Cormier, O. Majerus, D. R. Neuville, and G. Calas, Temperature-induced structural modifications between alkali borate glasses and melts, *J. Am. Ceram. Soc.* **89**, 13 (2006).
- [8] Q. Mei, C. J. Benmore, and J. K. R. Weber, Structure of Liquid SiO₂: A Measurement by High-Energy X-Ray Diffraction, *Phys. Rev. Lett.* **98**, 057802 (2007).
- [9] J. Kozaily, Structure et Dynamique d'aluminosilicates de Calcium Fondus, Ph.D. thesis, Université D'Orléans, Orléans, 2012.
- [10] O. Majerusa, L. Cormier, G. Calas, and B. Beuneu, A neutron diffraction study of temperature-induced structural changes in potassium disilicate glass and melt, *Chem. Geol.* **213**, 89 (2004).
- [11] L. Cormier, G. Calas, and B. Beuneu, Structural changes between soda-lime silicate glass and melt, *J. Non-Cryst. Solids* **357**, 926 (2011).
- [12] L. B. Skinner, C. J. Benmore, J. K. R. Weber, M. C. Wilding, S. K. Tumber, and J. B. Parise, A time resolved high energy x-ray diffraction study of cooling liquid SiO₂, *Phys. Chem. Chem. Phys.* **15**, 8566 (2013).
- [13] C. J. Benmore, J. K. R. Weber, M. C. Wilding, J. Du, and J. B. Parise, Temperature-dependent structural heterogeneity in calcium silicate liquids, *Phys. Rev. B* **82**, 224202 (2010).
- [14] L. Hennet, I. Pozdnyakova, A. Bytchkov, D. L. Price, G. N. Greaves, M. Wilding, S. Fearn, C. M. Martin, D. Thiaudiere, J. F. Berar, N. Boudet, and M. L. Saboungi, Development of structural order during supercooling of a Fragile oxide melt, *J. Chem. Phys.* **126**, 074906 (2007).
- [15] O. L. G. Alderman, C. J. Benmore, A. Tamalonis, S. Sendelbach, S. Heald, and J. K. R. Weber, Continuous structural transition in glass-forming molten titanate BaTi₂O₅, *J. Phys. Chem.* **120**, 26974 (2016).
- [16] P. K. Gupta and J. C. Mauro, The configurational entropy of glass, *J. Non-Cryst. Solids* **355**, 595 (2009).
- [17] F. H. Stillinger and P. G. Debenedetti, Glass transition thermodynamics and kinetics, *Annu. Rev. Condens. Matter Phys.* **4**, 263 (2013).
- [18] H. N. Ritland, Limitations of the fictive temperature concept, *J Am. Ceram. Soc.* **39**, 403 (1956).
- [19] I. M. Hodge, Effects of annealing and prior history on enthalpy relaxation in glass polymers. 6. Adam-Gibbs formulation of nonlinearity, *Macromolecules* **20**, 2897 (1987).
- [20] A. Ellison and I. A. Cornejo, Glass substrates for liquid crystal displays, *Int. J. Appl. Glass Sci.* **1**, 87 (2010).
- [21] P. K. Gupta and J. C. Mauro, The laboratory glass transition, *J. Chem. Phys.* **126**, 224504 (2007).
- [22] Y. Shi, D. Ma, A. P. Song, B. Wheaton, M. Bauchy, and S. R. Elliott, Structural evolution of fused silica below the glass-transition temperature revealed by in-situ neutron total scattering, *J. Non-Cryst. Solids* **528**, 119760 (2020).
- [23] R. C. Welch, J. R. Smith, M. Potuzak, X. Guo, B. F. Bowden, T. J. Kiczanski, D. C. Allan, E. A. King, A. J. Ellison, and J. C. Mauro, Dynamic of Glass Relaxation at Room Temperature, *Phys. Rev Lett.* **110**, 265901 (2013).
- [24] Certificate for Standard Reference Material 710a, Soda-lime-silica Glass, National Institute of Standards and Technology, Gaithersburg, MD 20899, USA (1991), https://www-s.nist.gov/srmors/view_cert.cfm?srm=710A.
- [25] O. Gulbitten, J. C. Mauro, X. Guo, and O. N. Boratav, Viscous flow of medieval cathedral glass, *J Am. Ceram. Soc.* **101**, 5 (2018).
- [26] J. Neuefeind, M. Feyngenson, J. Carruth, R. Hoffmann, and K. Chipley, The nanoscale ordered materials diffractometer NOMAD at the spallation neutron source SNS, *Nucl. Instrum. Methods Phys. Res. Sect. B* **287**, 68 (2012).
- [27] Y. Shi, N. T. Lonroth, R. E. Youngman, S. J. Rzoska, M. Bockowski, and M. M. Smedskjaer, Pressure-induced structural changes in titanophosphate glasses studied by neutron and X-ray total scattering analyses, *J. Non-Cryst. Solids* **483**, 50 (2018).
- [28] K. N. Trueblood, H.-B. Burgi, H. Burzlaff, J. D. Dunitz, C. M. Gramaccioli, H. H. Schulz, U. Shmueli, and S. C. Abrahams, Atomic displacement parameter nomenclature report of a subcommittee on atomic displacement parameter nomenclature, *Acta Crystallogr.* **A52**, 770 (1996).
- [29] Y. Shi, J. Neuefeind, D. Ma, K. Page, L. A. Lamberson, N. J. Smith, A. Tandia, and A. P. Song, Ring size distribution in silicate glasses revealed by neutron scattering first sharp diffraction peak analysis, *J. Non-Cryst. Solids* **516**, 71 (2019).
- [30] A. C. Hannon, Neutron diffraction techniques for structural studies of glasses, *Modern Glass Characterization* (Wiley, Hoboken, 2015), 195.
- [31] C. A. Angell, in *Relaxation in Complex Systems*, edited by K. L. Ngai and G. B. Wright, Naval Research Laboratory Report, 3, (1985).
- [32] S. Susman, K. J. Volin, D. G. Montague, and D. L. Price, Temperature dependence of the first sharp diffraction peak in vitreous silica, *Phys. Rev. B* **43**, 11076 (1991).
- [33] P. Vashishta, R. K. Kalia, and J. P. Rino, Interaction potential for SiO₂: A molecular-dynamics study of structural correlations, *Phys. Rev. B* **41**, 12197 (1990).
- [34] N. Mattern, H. Hermann, S. Roth, J. Sakowski, M. P. Macht, P. Jovari, and J. Jiang, Structural behavior of Pd₄₀Cu₃₀Ni₁₀P₂₀ bulk metallic glass below and above the glass transition, *Appl. Phys. Lett.* **82**, 2589 (2003).
- [35] K. D. Hammonds, M. T. Dove, A. P. Giddy, V. Heine, and B. Winkler, Rigid unit phonon modes and structural phase transitions in framework silicates, *Am. Mineral.* **81**, 1057 (1996).
- [36] M. G. Tucker, D. A. Keen, and M. T. Dove, A detailed structural characterization of quartz on heating through the α - β phase transition, *Mineral. Mag.* **65**, 489 (2001).
- [37] S. V. Nemilov, Physical ageing of silicate glasses at room temperature: General regularities as a basis for the theory and the possibility of a priori calculation of the ageing rate, *Glass Phys. Chem.* **26**, 511 (2000).
- [38] <http://energy.gov/downloads/doe-public-access-plan>.
- [39] <https://code.ornl.gov/mth/ts-tools>.